ISSN 1990-7931, Russian Journal of Physical Chemistry B, 2008, Vol. 2, No. 5, pp. 759–774. © Pleiades Publishing, Ltd., 2008.
Original Russian Text © S.M. Frolov, V.S. Aksenov, I.O. Shamshin, 2008, published in Khimicheskaya Fizika, 2008, Vol. 27, No. 10, pp. 5–21.

COMBUSTION AND EXPLOSION

Propagation of Shock and Detonation Waves in Channels with U-Shaped Bends of Limiting Curvature[1]

S. M. Frolov[a, b], V. S. Aksenov[a], and I. O. Shamshin[b]

[a] *Semenov Institute of Chemical Physics, Russian Academy of Sciences, Moscow, 119991 Russia*
[b] *Moscow Engineering Physics Institute (State University), Kashirskoe sh. 31, Moscow, 125080 Russia*
e-mail: smfrol@chph.ras.ru

Received March 15, 2007

Abstract—Systematic experimental and theoretical studies of the propagation of shock and detonation waves in cylindrical tubes and planar channels with two U-shaped bends of limiting curvature were performed. It was demonstrated that U-shaped bends substantially facilitate detonation initiation in gases. The minimum shock wave velocity required to initiate the detonation of a stoichiometric propane–air mixture under normal conditions in a near-critical diameter tube with two U-shaped bends of limiting curvature was found to be ~800 m/s.

DOI: 10.1134/S1990793108050187

INTRODUCTION

In the last 30–40 years, various aspects of the focusing of shock waves in inert and reactive media have been extensively studied [1–6], with most experimental and theoretical studies on detonation waves being performed in straight tubes [7]. At the same time, there are many situations where wave processes propagate in bent tubes.

Our experimental studies on the initiation and propagation of detonation waves in tubes with U-shaped bends, coils, and coil serpentines [8–12] demonstrated that such elements make it possible to substantially reduce the deflagration-to-detonation transition (DDT) distance and to decrease the critical intensity of the shock wave required to initiate detonation. Since this results are important for designing air-breathing pulse detonation engines (ABPDEs) [13], we proposed [8] and developed [11] the idea of using compact arrangements of detonation tubes with several U-shaped bends in such engines.

Such arrangement makes it possible to increase the length of the detonation tube without increasing the size of the installation. In addition, according to [8–12], U-shaped bends focus and amplify weak shock waves generated by a flame experiencing acceleration. At the same time, such bends increase the gasdynamic resistance and complicate the periodic filling of the tube with fresh combustible mixture. Thus, to construct compact ABPDEs, it is necessary to find a compromise solution.

In other words, the construction should be such as to ensure the onset of DDT within as short a time interval as possible. The DDT distance is known to decrease with the detonation tube diameter d. Note, however, that there is a minimum (critical) diameter of the tube $d = d_{\min}$ below which detonation is impossible. According to the data of various authors, $\lambda/\pi < d_{\min} < \lambda$, where λ is the transversal size of multifront detonation cell (for a stoichiometric propane–air mixture under normal conditions, $\lambda \approx 50$ mm).

The aim of the present work was to experimentally study the propagation of shock and detonation waves in near-critical tubes with two U-shaped bends and to numerically model the propagation of shock and detonation waves in a planar channel with bends of limiting curvature. The combustible mixture was a stoichiometric propane–air composition. That propane was chosen as the fuel was motivated by the fact that its detonatability is close to that of aviation kerosene [13].

EXPERIMENTAL SETUP

Figure 1 shows a schematic of the experimental setup; its main units are an initial shock wave generator and a detonation tube with two U-shaped bends. The initial shock wave generator (a propellant-driven gas generator (PDGG) or electric discharge generator (EDG)) was mounted on one of the end of the tube,

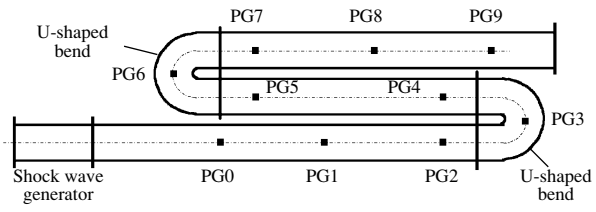

Fig. 1. Schematic of the experimental setup.

[1] Presented at XXXI Academic Readings on Astronautics, Moscow, January 2007.

Table 1. Positions of the pressure gages in the 51- and 41-mm-in-diameter detonation tubes

Experiment	$d = 51$ mm			$d = 41$ mm	
	PDGG	EDG	EDG-A	PDGG	EDG
PG0	400	0	850	450	0
PG1	650	650	1310	750	750
PG2	900	900	1810	1050	1050
PG3	1140	1140	2050	1335	1335
PG4	1380	1380	2726	1590	1590
PG5	1816	1816	2966	1953	1953
PG6	2056	2056	3206	2241	2241
PG7	2296	2296	3506	2494	2494
PG8	2596	2596	3806	2794	2794
PG9	2896	2896	–	3294	3294

whereas the other end was closed. The experiments were performed with smooth tubes with internal diameters of 51 and 41 mm and bends of limiting curvature, which, in contrast to the previous experiments [8, 11, 12]) made the installation more compact. The bends were made of four segments of a tube using electric welding. The internal radius of the bends was $R = 11 \pm 1$ mm. Before each experiment, the tube was evacuated and then filled with a stoichiometric propane–air mixture to atmospheric pressure (0.1 MPa); the initial temperature was 293 ± 2 K.

The pressure profiles and the velocity of shock waves in the tubes were measured with LKh600 pressure gages (PG0–PG9). The distances from the shock wave generator to the pressure gages are listed in Table 1. To monitor the onset of the detonation regime, photodiodes were installed near some of the pressure gages (in the same sections), which recorded the luminescence of the detonation products. The signals from the pressure gages and photodiodes were fed into an analog-to-digital converter (L-Card L-783) and processed by a computer. In addition, a smoked plate was installed in the outlet section of the tube to identify detonation through the imprints it left.

The mean velocity of the shock wave over each measurement segment was determined from the distance between the gages and the time it took for the wave to cover it as measured from the pressure oscillograms for each gage. The error in determination of the mean velocity was within 3%.

The PDGG was a 22-cm^3 cylindrical chamber equipped with a changeable flow-control nozzle and membrane unit. The gas generator was operated with a 1.5- to 2.25-g porous pyroxylin propellant charge. The charge was initiated with a pyrotechnical ignitor. The propellant-driven gas generator made it possible to generate shock waves with a prolonged compression phase, since the duration of propellant burning was 1 to 2 ms. The use of membranes of various thicknesses and prepared from different materials made it possible to vary the maximum pressure in the gas generator and, hence, the initial velocity of the primary shock wave.

The EDG was a three-electrode discharger. The trigger discharge produced a hot gas volume (plasma) near the main-discharge electrodes. The distance between the main electrodes was 8 mm, whereas the distance between the trigger and main electrodes was 3 mm. The energy of the trigger discharge was constant (≈57 J), whereas the main discharge energy was varied from 0.9 to 2.5 kJ. The capacity of the main discharge capacitors was constant 800 μF, whereas the charge voltage was varied within 1.5–2.5 kV. The characteristic discharge time was 20–40 μs. In contrast to the PDGG, the EDG generated a shock wave with a very short compression phase. The initial velocity of the primary shock wave was varied by changing the voltage across the discharge capacitor of the EDG. In addition, we performed experiments with an elongated tube, with an 850-mm additional section, which was installed between the discharger and the first straight section of the detonation tube (Table 1) The experiments performed with the use of the additional section will be referred to as EDG-A.

Thus, we varied the detonation tube diameter, initial shock wave velocity, and compression phase duration of the initial shock wave.

EXPERIMENTAL RESULTS

Table 2 lists the mean velocities (km/s) of the shock waves generated by the PDGG and EDG in detonation tubes of different diameters. Figures 2 and 3 show the relative velocity of the shock wave as a function of the distance along the detonation tube axis. The measured shock wave velocity was normalized by the CJ detonation velocity of a stoichiometric propane–air mixture ($D_0 \approx 1800$ m/s). The two dashed vertical lines in Figs. 2 and 3 mark the positions of the U-shaped bends (gages PG2 and PG6, respectively). For example,

Table 2. Shock wave velocities (km/s) recorded at different measurement segments (the numbers of rows correspond to the numbers of the curves in Figs. 2 and 3)

No.	PG0–PG1	PG1–PG2	PG2–PG3	PG3–PG4	PG4–PG5	PG5–PG6	PG6–PG7	PG7–PG8	PG8–PG9
Tube with d = 51 mm (PDGG)									
1	0.84	0.73	0.73	0.60	0.64	0.63	0.52	0.75	1.07
2	0.90	0.78	0.77	0.61	0.58	0.63	0.50	0.55	0.53
3	0.84	0.83	0.80	0.70	0.79	1.19	1.52	1.91	1.83
4	0.96	0.94	0.94	0.87	1.56	1.86	1.53	1.83	1.73
5	1.28	1.12	1.12	0.88	0.79	0.84	0.65	0.72	0.68
6	1.98	1.74	1.62	1.52	1.66	1.65	1.44	1.80	1.64
7	1.89	1.72	1.70	1.49	1.62	1.55	1.47	1.69	1.64
8	0.86	0.84	0.87	0.77	1.23	1.19	1.56	1.80	1.73
Tube with d = 51 mm (EDG)									
1	0.94	0.70	0.65	0.53	0.57	0.54	0.46	0.51	0.49
2	1.09	0.76	0.69	0.56	0.53	0.56	0.46	0.51	0.49
3	1.23	0.79	0.72	0.58	0.57	0.59	0.49	0.54	0.52
4	1.20	0.80	0.74	0.61	0.80	0.75	0.90	1.13	1.11
5	1.33	0.90	0.83	0.65	0.98	1.11	1.38	1.80	1.70
6	1.84	1.69	1.73	1.41	1.59	1.65	1.39	1.59	1.59
7	1.96	1.62	1.78	1.44	1.63	1.69	1.39	1.67	1.56
Tube with d = 51 mm (EDG-A)									
1	0.86	0.78	0.74	0.64	0.64	0.51	0.57	0.51	–
2	0.95	0.89	0.79	0.44	0.44	0.75	0.77	1.34	–
3	1.75	1.70	1.6	1.21	1.04	0.93	1.16	1.03	–
4	1.64	1.70	1.63	1.62	1.49	1.49	1.71	1.65	–
5	1.73	1.70	1.71	1.61	1.61	1.48	1.75	1.65	–
Tube with d = 41 mm (PDGG)									
1	0.52	0.74	0.68	0.59	0.66	0.58	0.52	0.58	0.55
2	0.88	0.83	0.75	0.67	0.73	0.66	0.92	1.95	1.85
3	0.71	0.84	0.81	0.71	0.93	1.50	1.72	1.86	1.83
4	0.76	0.92	0.86	0.89	1.42	1.82	1.61	1.78	1.76
5	0.90	1.13	0.99	1.82	1.79	1.72	1.56	1.74	1.74
6	0.83	1.10	1.07	1.82	1.95	1.68	1.57	1.78	1.76
7	1.53	1.78	1.54	1.52	1.88	1.62	1.50	1.67	1.77
Tube with d = 41 mm (EDG)									
1	0.93	0.79	0.61	0.64	0.67	0.60	0.54	0.61	0.67
2	1.03	0.89	0.68	0.71	0.71	0.67	0.58	1.19	1.30
3	1.18	0.97	0.78	0.93	0.98	1.01	1.77	1.86	1.80
4	1.15	0.98	0.81	0.96	0.90	0.97	1.07	2.04	1.80
5	1.12	0.97	0.85	1.01	1.04	1.02	1.76	1.86	1.77
6	1.74	1.71	1.51	1.58	1.76	1.55	1.57	1.71	1.74
7	1.70	1.71	1.56	1.58	1.73	1.64	1.54	1.74	1.74

curve *5* in Fig. 2a illustrates the attenuation of a shock wave generated by the PDGG in the 51-mm tube filled with air.

It was revealed that there is a minimum shock wave velocity at the entrance into the first U-shaped bend (the mean velocity over the PG2–PG3 base) above which

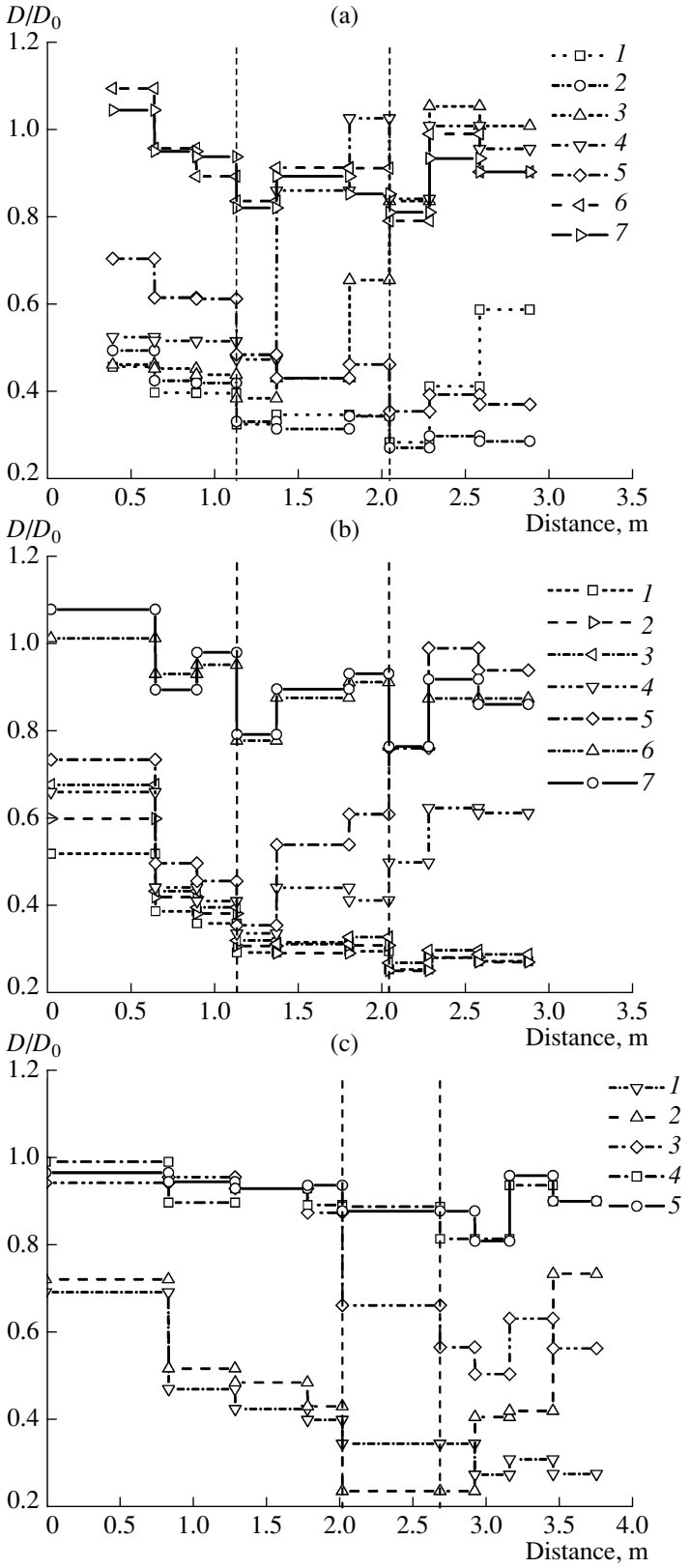

Fig. 2. Mean shock wave velocity at various measurement segments of the 51-mm-in-diameter tube: (a) PDGG, (b) EDG, and (c) EDG-A (the tube with an additional section). The numbers of the curves correspond to the numbers of the rows in Table 2. The symbols are used to identify the curves.

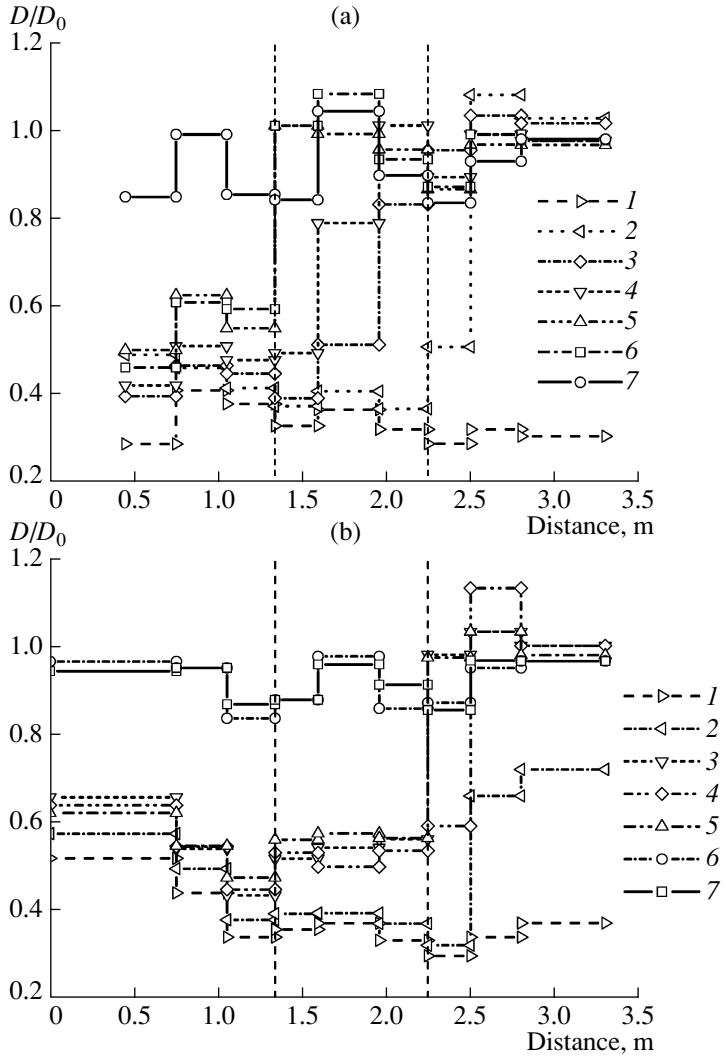

Fig. 3. Mean shock wave velocity at various measurement segments of the 41-mm-in-diameter tube: (a) PDGG and (b) EDG. The numbers of the curves correspond to the numbers of the rows in Table 2. The symbols are used to identify the curves.

detonation arises within the straight section behind the second U-shaped bend. For shock waves in the 51-mm tube generated by the PDGG and EDG, $D_{min} \approx 800$ m/s (Fig. 2a, curve *3*) and 830 m/s (Fig. 2b, curve *5*); for shock waves in the 41-mm tube generated by the PDGG and EDG the velocities were lower, $D_{min} \approx$ 750 m/s and 780 m/s (Fig. 3a, curve *2* and Fig. 3b, curve *3*). At shock wave velocities within 750–800 m/s, detonation arose behind the second U-bend; at shock wave velocities within 850–940 m/s, it arose behind the first U-shaped bend (Fig. 2a, curve *4* and Fig. 3a, curve *5*). Here, the first and second values refers to the 41- and 51-mm tubes, respectively. For comparison, it is worthwhile to note that for a 51-mm tube with one U-bend of larger diameter (R = 51 mm), detonation was observed only at a primary shock wave velocity of more than 1100 m/s [8, 11, 12]. Note also that detonation in 51- and 41-mm straight tubes was initiated by shock waves with velocities within 1700–1800 m/s.

Figures 4 and 5 show typical recordings of the pressure for the onset of detonation in 51- and 41-mm bent tubes behind the second U-bend, which correspond to curve *8* in Fig. 2a and curve *2* in Fig. 3a. In these experiments, the velocities measured over the PG7–PG8 and PG8–PG9 bases were close to the detonation velocity. At the positions of the PG7–PG8 gages, the signals from the photodiodes deviated sharply from the base line simultaneously with the signals from these pressure gages, observations indicative of the formation of a detonation wave, with a reaction zone behind its front. The soot imprints obtained clearly showed the trajectories of triple points, which formed a cellular structure with a cell width close to the tube diameter. All the data obtained are indicative of the onset of the detonation regime. That the measured detonation velocity was somewhat lower the CJ velocity (Table 2) can be accounted for by momentum and energy losses in tubes with near-critical diameter.

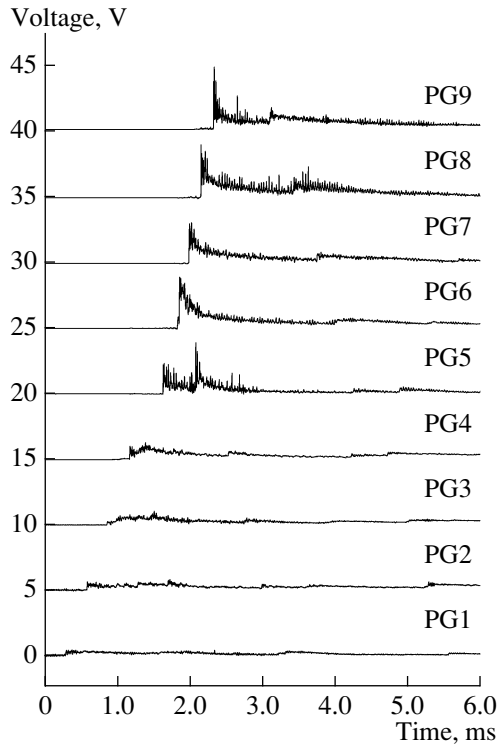

Fig. 4. Pressure oscillograms for the experiment in which detonation was initiated after the second U-bend of the 51-mm tube with the PDGG (Fig. 2a, curve *8*).

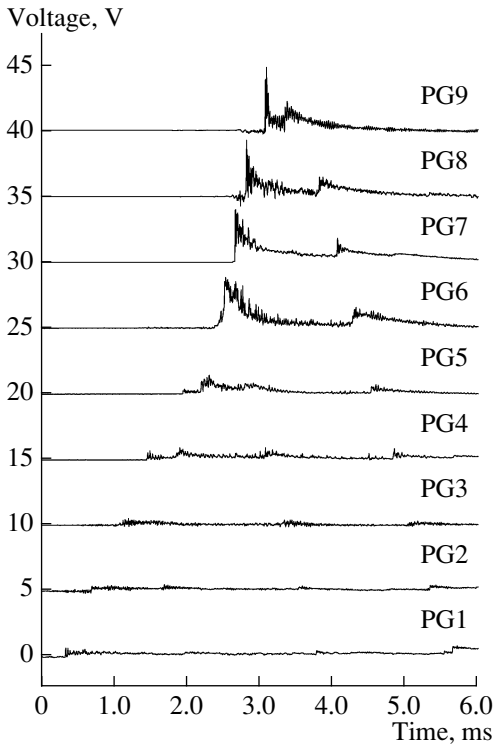

Fig. 5. Pressure oscillograms for the experiment in which detonation was initiated after the second U-bend of the 41-mm tube with the PDGG (Fig. 3a, curve *2*).

At shock wave velocities of $D < D_{min} \approx 800$ m/s, no detonation was observed (see, e.g., Fig. 2a, curve *2*), although pressure gages recorded secondary explosions behind the primary shock wave. When passing a U-bend, a planar shock wave reflected from the external wall, a process that might initiate self-ignition of the mixture with its subsequent combustion and shock wave strengthening. The acceleration of the shock wave caused by a partial burnout of the explosive mixture was observed in the 51-mm PDGG-driven tube at a shock wave velocity of ~730 m/s at the entrance into the first U-bend (Fig. 2a, curve *1*), in the 51-mm EDG-driven tube at a shock wave velocity of ~740 m/s (Fig. 2b, curve *4*), in the 51-mm EDG-driven tube with additional section at a shock wave velocity of ~750 m/s (Fig. 2c, curve *2*), and in the 41-mm EDG-driven tube at a shock wave velocity of ~680 m/s (Fig. 3b, curve *2*).

By analogy with the critical phenomena observed during detonation initiation in straight tubes, the above effects should also be treated as critical for tubes with U-bends. It cannot be excluded that, if the length of the straight section behind the second U-bend was increased or if the length of the straight section between the two U-bends was changed, detonation might arise, all other things being equal. Note also that, near the detonatability limit, hysteresis phenomena were observed. In run no. 1 (Table 2, 51-mm EDG-driven tube), the shock wave velocity at the entrance into the first U-bend was ~730 m/s, whereas the velocity at the exit of the second U-bend (measured over the PG8–PG9 base) was 1070 m/s. In run no. 2 (Table 2, the 51-mm EDG-driven tube), the shock wave velocity decreased monotonically from ~770 m/s at the entrance into the first U-bend to 530 m/s at the exit of the second U-bend.

To directly initiate detonation in a 51-mm straight tube with the EDG, it was necessary to generate a strong primary shock wave, $D \approx 1900$–2000 m/s (PG0–PG1; curves *6* and *7* in Fig. 2a). As the wave propagated through the straight section to the first U-bend, its velocity decreased to 1700–1750 m/s ($\approx 0.96D_0$) at its entrance. As the shock wave traveled through the U-bends, its velocity decreased to ~1520 m/s ($0.84D_0$) in the first bend and to ~1490 m/s ($0.82D_0$) in the second bend. After passing the bends, the wave increased its velocity to 1640–1800 m/s (0.91–$1.00D_0$).

A similar behavior was observed in the 51-mm EDG-driven tube (curves *6* and *7* in Fig. 2b) and the 51-mm EDG-A-driven tube, with the only difference that the drops in the velocities of the shock wave in the U-bends were higher, up to $0.77D_0$. In experiments on the EDG-A-driven tube, regimes with attenuation of strong shock waves, without the repeated initiation of detonation, were observed. For example, curve *3* in Fig. 2c corresponds to the case where the shock wave velocity decreased from 1600 m/s before the first

U-bend to 1210 m/s (≈0.67D_0) after and to 1040 m/s (≈0.58D_0) after the second U-bend.

MODEL

The problem of propagation of a shock wave through a U-shaped bend of a cylindrical tube involves solving 3D gasdynamics equations. To gain insights into detonation initiation in bent tubes, we simulated the propagation of shock waves in planar channels with two U-bends with geometric parameters identical to those realized in physical experiments. Since the characteristic times of the processes under study are rather small (hundreds of microseconds), there is no need to take into account viscosity and heat transfer. Therefore, the model included only the equations of conservation of mass, momentum, and energy for an ideal multicomponent nonviscous and non-heat-conducting gas (Euler equations). In the Cartesian coordinate system, these equations can be written in the following vector form:

$$\frac{\partial \mathbf{U}}{\partial t} + \frac{\partial \mathbf{F}}{\partial x} + \frac{\partial \mathbf{G}}{\partial y} = \mathbf{S} \quad (1)$$

with

$$\mathbf{U} = \begin{bmatrix} \rho \\ \rho u \\ \rho v \\ \rho E \\ \rho Y_i \end{bmatrix}, \quad \mathbf{F} = \begin{bmatrix} \rho u \\ \rho uu + p \\ \rho uv \\ (\rho E + p)u \\ \rho Y_i u \end{bmatrix},$$

$$\mathbf{G} = \begin{bmatrix} \rho v \\ \rho uv \\ \rho vv + p \\ (\rho E + p)v \\ \rho Y_i v \end{bmatrix}, \quad \mathbf{S} = \begin{bmatrix} 0 \\ 0 \\ 0 \\ Q \\ J_i \end{bmatrix}.$$

Here, ρ is the gas density; u and v are the velocity vector components; E is the total specific energy of the gas; p is the pressure; Y_i is the mass fraction of ith component in the gas mixture; J_i is the rate of formation (consumption) of ith component; Q is the rate of heat release by the chemical reactions; and N_g is the number of components in the gas mixture.

The total specific energy of the gas is given by

$$E = e + \frac{1}{2}(u^2 + v^2),$$

where e is the specific internal energy of the gas,

$$e = \int_0^T C_v(T)dT = \bar{C}_v(T)T.$$

Here, $C_v(T)$ is the specific heat at constant volume, $\bar{C}_v(T)$ is the mean specific heat for the temperature range from 0 to T, and T is the gas temperature.

The specific heat of the gas $C_v(T)$ was calculated using the specific heats of the components:

$$C_v(T) = \sum_{i=1}^{N_g} Y_i C_{vi}(T).$$

The temperature dependences of the specific heats of the components were presented in the form of a fourth-order polynomial [14]:

$$C_{vi}(T)/R = A_{1,i} + A_{2,i}T + A_{3,i}T^2 + A_{4,i}T^3 + A_{5,i}T^4.$$

The above equations (1) were supplemented with the equation of state of an ideal gas:

$$p = \rho RT \sum_{i=1}^{N_g} Y_i \mu_i^{-1}, \quad (2)$$

where μ_i is the molecular weight of the ith component and R is the universal gas constant.

The specific internal energy and equation of state (2) were used to determine the thermodynamic characteristics of the system, temperature T and pressure p. The problem was closed using the initial and boundary conditions presented below.

The chemical transformations were described by a set of N_r irreversible chemical reactions:

$$\sum_{i=1}^{N_g} \nu'_{ik} A_{ik} \xrightarrow{k} \sum_{j=1}^{N_g} \nu''_{jk} B_{jk},$$

where A_{ik} are the initial reactants, B_{jk} are the gaseous products of kth reaction, and ν'_{ij} and ν''_{jk} are the stoichiometric coefficients. The reaction rate was presented as

$$w_k = A_k T^{n_k} (P/P_0)^{m_k} \exp(-(E_a)_k/(RT)) \times \prod_{i=1}^{N_g} (\rho Y_i/\mu_i)\,\mathrm{sgn}(\nu'_{ik}), \quad (3)$$

where A_k is the preexponential factor, $(E_a)_k$ is the activation energy, n_k is the effective reaction order, m_k is a parameter that describes the pressure dependence of the reaction rate, and P_0 is the atmospheric pressure. Based on the known reaction rates, the quantities Q and J_i were presented as

$$Q = \sum_{k=1}^{N_r} w_k Q_k, \quad Q_k = \sum_{i=1}^{N_g} (\nu'_{ik} - \nu''_{ik}) \Delta H_i^0,$$

$$J_i = \sum_{k=1}^{N_r} (\nu''_{ik} - \nu'_{ik}) \mu_i w_k,$$

where Q_k is the heat effect of the kth reaction and ΔH_i^0 are the standard enthalpies of formation of the substances.

In preliminary calculations, the oxidation of propane was modeled using a five-step overall kinetic mechanism [15]:

$$C_3H_8 + 3.5O_2 \longrightarrow 3CO + 4H_2O,$$
$$2CO + O_2 \longrightarrow 2CO_2,$$
$$CO + H_2O \longrightarrow CO_2 + H_2,$$
$$CO_2 + H_2 \longrightarrow CO + H_2O,$$
$$2H_2 + O_2 \longrightarrow 2H_2O.$$

Since calculations with this mechanism were time-consuming, we performed simplified calculations with the one-step mechanism of propane oxidation:

$$C_3H_8 + 5O_2 \longrightarrow 3CO_2 + 4H_2O. \quad (4)$$

It turned out that the simulation results obtained with the use of the five- and one-step differed little; therefore, all calculations were performed using the one-step mechanism. The rate of reaction (4) was calculated by formula (3), as for a bimolecular reaction of propane with oxygen. We used the following kinetic parameters: $A_1 = 7 \times 10^8$ m^3/(mol s), $n_1 = 0$, $m_1 = -0.2264$, and $(E_a)_1 = 191$ kJ/mol. This values were obtained by processing experimental data on ignition delay times [16, 17], with consideration given to the fact that the transversal size of the detonation cell for the stoichiometric propane–air mixture under normal conditions is close to 50 mm. The heat effect of the reaction calculated from the enthalpies of formation of the reactants and products of reaction (4) was found to be 46.6 MJ per kg of propane.

Thermodynamic calculations of the detonation velocity in a propane–air mixture, performed using the TDS code [18], yielded 1800 m/s and 1910 m/s, respectively, when the equilibrium composition of the detonation products was used and when only C_3H_8, O_2, N_2, CO_2, and H_2O (reactants and products of reaction (4)) were taken into account.

NUMERICAL METHOD

The model equations were solved by using the principle of separation of physical processes [19]. According to this principle, at each time step, the effects of convective transfer and pressure work are first treated, after which the effect of chemical transformations is taken into account.

At the first stage, we solved the system of equations

$$\frac{\partial \mathbf{U}^*}{\partial t} + \frac{\partial \mathbf{F}}{\partial x} + \frac{\partial \mathbf{G}}{\partial y} = 0 \quad (5)$$

by the Godunov method [20]. To numerically realize the boundary conditions, the dummy-cell method was used. The fluxes of mass, momentum, and energy at the boundaries of the cells were determined from the exact solution to the Riemann problem. The initial parameters for the Riemann problem were calculated at the boundary of the cell on the premise that the parameters inside the cells are distributed linearly, in accordance with the principle of minimum derivative increment [21]. Thus, the second-order accuracy of the difference scheme in the spatial coordinates was attained. The boundary condition was formulated in the form of the channel wall impermeability to substances. In the sweep scheme, this was achieved by setting the normal velocity at the boundary equal to zero.

At the second stage, we solved the system of differential equations

$$\frac{\partial \mathbf{U}}{\partial t} = \mathbf{S}(\mathbf{U}^*), \quad (6)$$

which describes the gas composition change and the energy release by the chemical transformations. The input data in solving system (6) were the results of numerical solution of system (5). System (6) was solved numerically using the fourth-order Runge–Kutta explicit method [22]. In some cases, to test the accuracy of the algorithm, the implicit method was employed [23], which was developed especially for integrating chemical kinetics equations. Test calculations revealed no appreciable distinctions.

The time step size was chosen according to the Courant condition:

$$\Delta t^{CFL} = K \frac{\min\limits_{i,j} (\Delta x_i, \Delta y_j)}{\max\limits_{i,j} (|u_{i,j} \pm c_{i,j}|, |v_{i,j} \pm c_{i,j}|)},$$

where K is the Courant number. All calculations were performed with $K = 0.1$. To enhance the stability of calculations in passing from one time layer to the next, we allowed only small variation in the step, using the following heuristic rule:

$$\Delta t^{n+1} = \begin{cases} \min(\Delta t^{CFL}, (1+\alpha)\Delta t^n), & \Delta t^n \le \Delta t^{CFL} \\ \max(\Delta t^{CFL}, (1-\alpha)\Delta t^n), & \Delta t^n > \Delta t^{CFL}, \end{cases}$$

where α is a small constant, 0.1–0.3. The difference analogue of the governing equations was presented in [24].

The accuracy of the numerical method was preliminary tested on standard problems for the decay of an arbitrary discontinuity and on problems describing the diffraction of shock waves on a wedge. In preliminary calculations, we examined the effects of all numerical parameters, including the computational cell size, on the results.

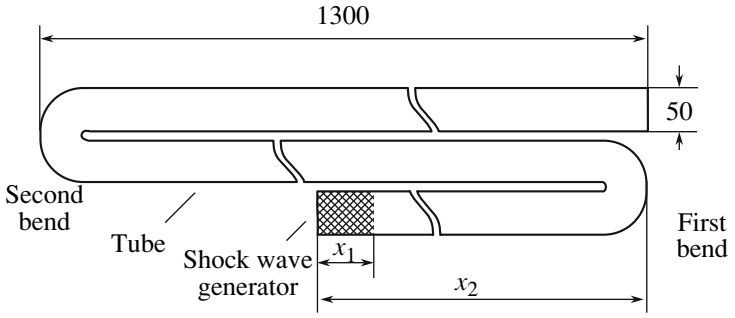

Fig. 6. Schematic of the computational domain.

CALCULATION RESULTS

Calculations were performed on a planar uniform rectangular grid with a computational cell size of 0.5 mm. Figure 6 shows a scheme of the computational domain, which imitates the 51-mm tube with two U-bends that was used in physical experiments. As in the experimental setup, the planar channel had three straight sections and two U-shaped bends of limiting curvature. The height of the channel and the middle section length were 50 and 1200 mm, respectively.

At the initial moment of time, the entire channel was uniformly filled with stoichiometric propane–air mixture. The primary shock wave was generated in an initiation section of length x_1. In this section, the pressure, temperature, and mixture velocity were such as to ensure the required Mach number of the shock wave $M_0 = D/c_0$, where c_0 is the speed of sound in the unperturbed fresh mixture. The parameters of the mixture in the main section were $p = 0.1$ MPa and $T = 298$ K.

When performing calculations, we varied the primary shock wave intensity M_0 and the compression phase duration τ_+ at the entrance into the first U-bend. At a given shock wave intensity, the compression phase duration was determined by the initiation section length x_1 and distance to the bend $x_2 - x_1$. The inset in Fig. 7 illustrates how the value of τ_+ was determined from the calculated pressure profile.

Figure 7 shows the calculated parametric regions of detonation existence in the M_0–τ_+ plane. The closed symbols represent calculations according to which a detonation wave emerged after the first bend, whereas the open symbols signify no detonation conditions. Circles and squares refer to experiments with U-bends of limiting curvature and with bends of smaller curvature ($R = H$ [12]) (Fig. 6). The curves approximating the critical condition of detonation onset after the first U-shaped bend (τ_+ in ms):

$$M_0 = 3.5 + 400\tau_+^{-2}$$

for the limiting curvature bend (solid line in Fig. 7) and

$$M_0 = 3.55 + 22\tau_+^{-0.9}$$

for the bend with a curvature equal to the channel width (dashed line). The onset of detonation was observed only above these curves.

The maximum value of τ_+ in calculations was 1.1 ms (the corresponding points in Fig. 7 are not shown). As can be seen from Fig. 7, starting from $\tau_+ = 0.2$–0.3 ms, the curves level off onto a horizontal plateau; i.e., a further increase in the compression phase duration produces no noticeable effect on the minimum shock wave intensity required to initiate detonation. Note that, in the limiting curvature tube, detonation appeared at smaller values of M_0 and τ_+. It is this circumstance that prompted us to study detonation in tube with U-shaped bends of limiting curvature.

Figure 8 shows typical calculation results for four variants, as examples. It displays the maximum pressure at each point of the channel over the entire observation time, so-called numerical soot imprints. The compression phase duration for the variants presented in Fig. 8a and 8b was $\tau_+ = 0.3$ ms, while that for the variants shown in Figs. 8c and 8d was $\tau_+ = 0.06$ ms. The corresponding values of the shock wave velocity at the entrance into the first U-bend are $D = 1180$ (Fig. 8a), 1215 (Figs. 8b and 8c), and 1325 m/s (Fig. 8d) or 3.48, 3.58, and 3.91 in terms of the Mach number.

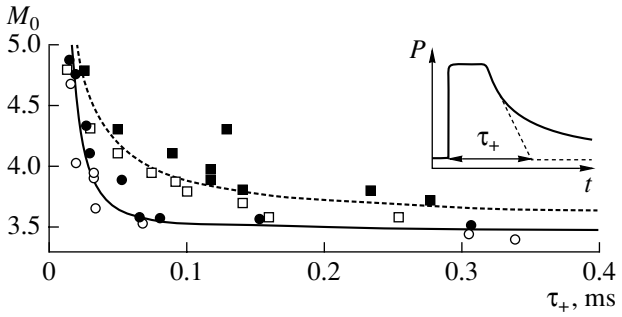

Fig. 7. Calculated detonation initiation regions for 51-mm tubes with U-bends of different curvatures: (○/□) no detonation, (●/■) detonation, (○/●) channel with U-bends of limiting curvature, (□/■) channel with U-bends of radius $R = H$. The curves approximate the critical condition of detonation initiation. The inset shows how the compression phase duration τ_+ of the shock wave was determined.

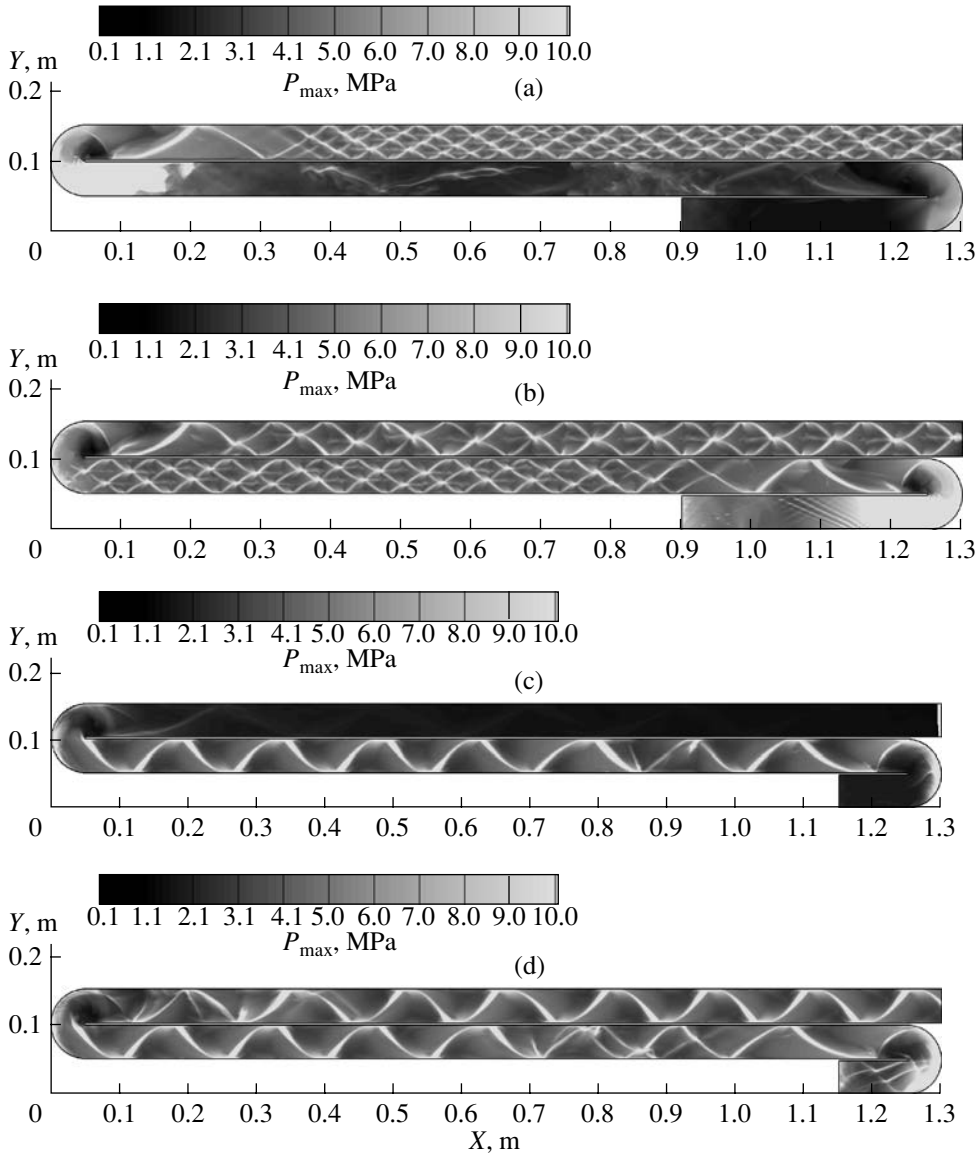

Fig. 8. Calculated maximum pressure fields ("numerical soot imprints"): τ_+ = (a, b) 0.3 ms and (c, d) 0.06 ms. The shock wave velocity at the entrance into the U-bend was (a) 1180, (b, c) 1215, and (d) 1325 m/s.

For the same variants, the dependences of the relative shock wave velocity on the distance traveled along the channels with two U-bends (D_0 = 1910 m/s) are displayed in Fig. 9. The origin of the distance was set at the entrance into the first U-bend. The velocity was determined by analyzing the pressure evolution at points located at the axis of the channel. The pressure in the U-bends was monitored at 15 points.

Under the condition corresponding to Fig. 8a (D = 1180 m/s), the maximum temperature in the shock wave reflected from the external wall of the first U-bend was high enough to initiate the self-ignition of the mixture, but the size of the hotspot was too small to ensure the coupling of the shock wave front and the reaction behind it (according to the terminology accepted in [25]), and, therefore, the reaction zone lagged behind the shock wave. Nevertheless, chemical transformations behind the shock wave occurred and generally accelerated the shock wave: at the entrance into the second U-bend its velocity was already as high as 1300 m/s. In addition, the compression phase duration of the shock wave increased due to energy release behind the front. The new parameters of the shock wave proved high enough to ignite the mixture in a large volume practically instantaneously (within 1–2 μs) upon reflection from the second U-bend. This local secondary explosion resulted in the formation of two secondary shock waves, downstream and upstream. After several reflections from the channel wall at a distanse of 5H to 6H, the downstream shock wave transformed into a overdriven detonation wave, which propagated up to

the outlet without appreciable changes in the mean velocity (Fig. 9a, curve *1*) and cellular structure (Fig. 8a).

Under the conditions specified in Fig. 8b (D = 1215 m/s), the passage of the shock wave through the first U-bend produced a detonation wave. When it passed through the second U-bend, its cellular structure was first destroyed and then recovered at a distance of (5–6)H. The numerical soot imprint displayed in Fig. 8b is similar to imprints obtained in numerical simulations of the propagation of detonation in channels with partial obturation [26]: first, the flow converges and then expands, thereby producing an inclined shock wave, which then transforms into a detonation wave.

Under the conditions characteristic of Fig. 8c (D = 1215 m/s), when the compression phase was shorter than in the case presented in Fig. 8b, detonation with a single transverse wave arose and propagated behind the first U-bend. When passing the second U-bend, it decayed into a shock wave and a reaction zone lagged behind; this can be explained by the interaction of the transverse wave with a rarefaction wave at the internal wall of the bend. As the shock wave velocity was increased from 1215 to 1325 m/s (Fig. 8d), the instant of arrival of the shock wave at the second U-bend somewhat, and the detonation wave successfully passed through it.

Figure 9a suggests that shock waves with a relatively large compression phase produced detonation behind the first U-band at D = 1215 m/s (D/D_0 = 0.64, curve *2*) and only behind the second U-bend at D = 1180 m/s (D/D_0 = 0.62, curve *1*). This result is in agreement with experimental data. At a short compression phase duration (Fig. 9b), a shock wave with the same initial velocity (D = 1215 m/s, D/D_0 = 0.64; curve *1*) failed to initiate detonation behind the second U-bend—only at D = 1325 m/s (D/D_0 = 0.69, curve *2*), it did. Under the conditions specified in Figs. 9a and 9b, the velocity of a shock wave propagating through the first U-bend changed identically: first increased to D/D_0 = 1.5 at the center of the bend and then decreased to D/D_0 = 0.2 at exit from the bend. The subsequent sharp increase in the shock wave velocity to D/D_0 = 1.6–2.0 at the exit from the bend (Fig. 9a, curve *2*) is caused by secondary explosions near the external wall of the bend and by the interference of the reflected second explosion waves with the primary shock wave.

The distinctions in the detonation wave structures displayed in Fig. 8 can be accounted for by the number of secondary explosions initiated by the shock wave when it passes through the U-bends. For example, the structures of the long waves (Fig. 8a and 8b) are represented by two or three transverse waves generated by several secondary explosions, whereas the structures of the short waves, by one transverse wave. This behavior clearly manifests itself for the diffraction of waves in the second U-bend: the short wave did not survive the cooling action of the centered rarefaction wave originated at the internal wall of the bend, whereas the long

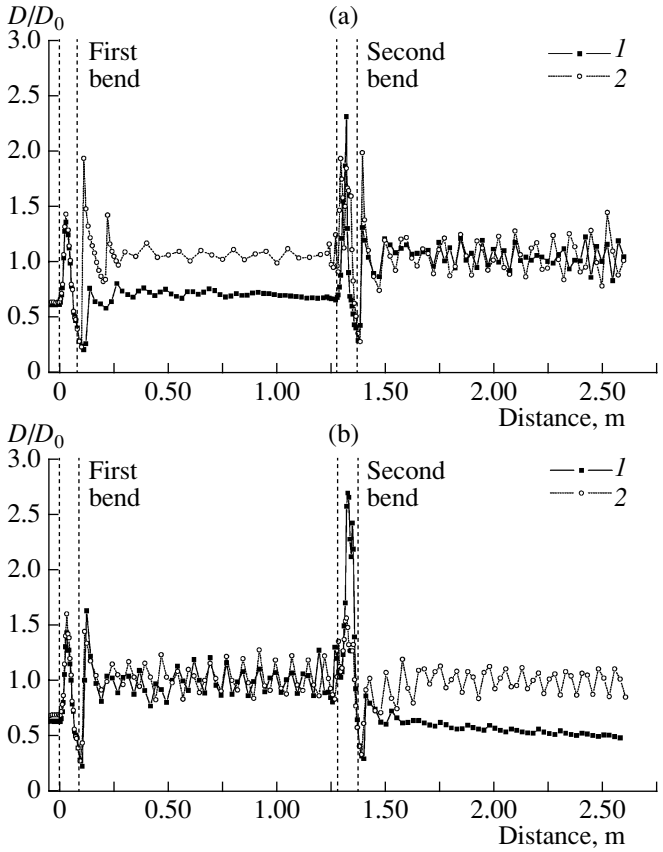

Fig. 9. Calculated dependences of the shock wave velocity on the distance traveled along the axis of the channel: τ_+ = (a) 0.3 ms ((*1*) D = 1180 m/s, (*2*) 1215 m/s) and (b) 0.06 ms ((*1*) D = 1215 m/s, (*2*) 1325 m/s).

wave did. The passage of the shock wave through the second U-bend is characterized by very high velocities, D/D_0 = 2.0–2.7. Averaging of the calculated velocity at three points (at the entrance, center, and exit from the bend) yields a value close to the velocity measured experimentally, D/D_0 = 1.2. Note that within the straight sections of the channel, detonation waves propagated at approximately mean velocities equal to the detonation velocity ($D/D_0 \approx 1$) irrespective of the wave structure (Figs. 9a and 9b).

Numerical calculations demonstrated the flow that arises during the propagation of a shock wave through a U-bend has a complicated structure. Figures 10–13 show the results of two sets of calculations in the form of pressure and density fields at various moments of time, as an example. According to the first set of calculations (Figs. 10 and 11), no detonation arises behind the bend. The second set of calculations (Figs. 12 and 13) is indicative of detonation onset. The conditions of the calculations differed only in the initial shock wave velocity: D = 1175 m/s in the first set of calculations and D = 1200 m/s in the second set. In other words, these two sets of calculations corresponded to the tran-

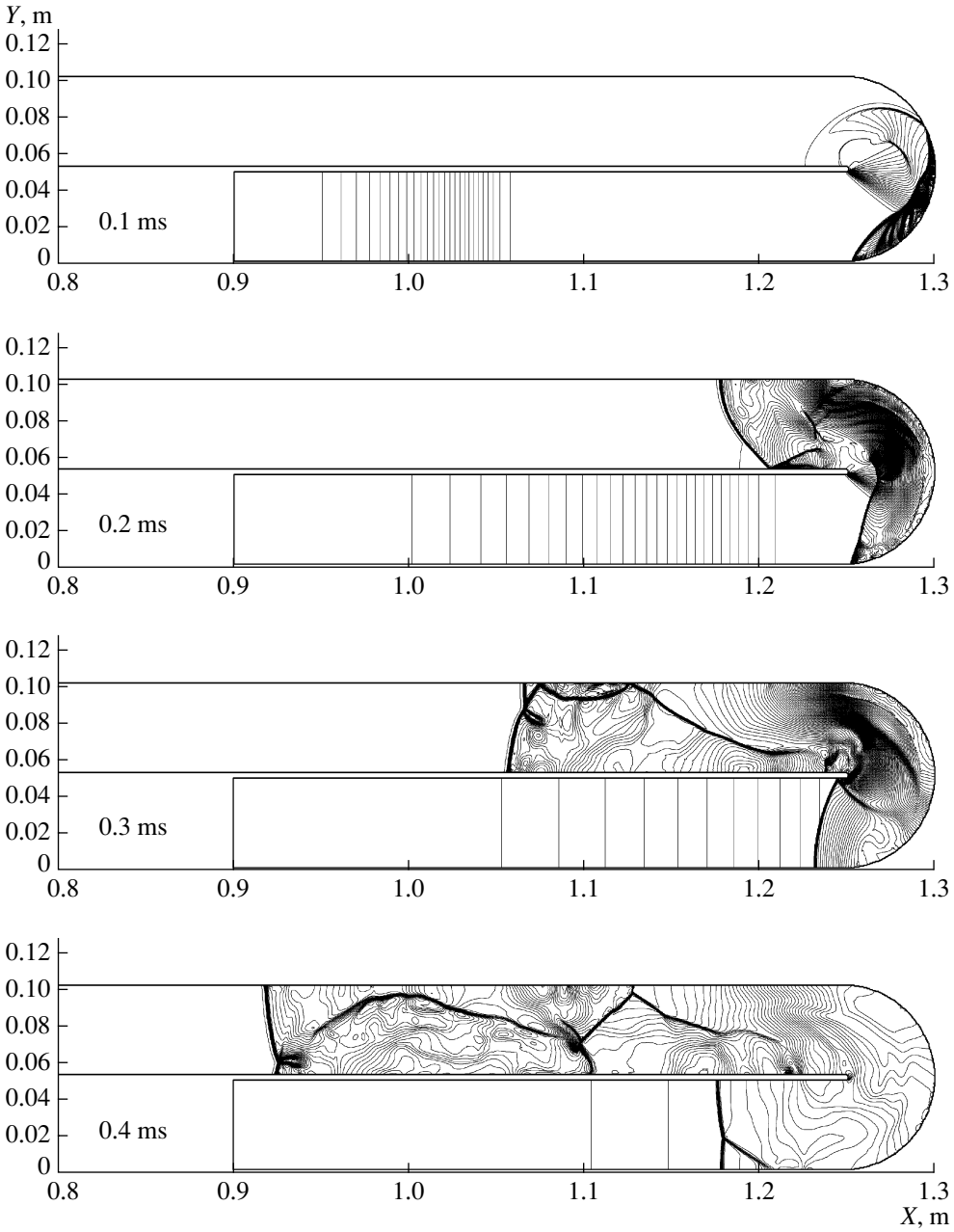

Fig. 10. Calculated pressure isolines at D = 1175 m/s and τ_+ = 0.3 ms.

sition over the critical condition of detonation initiation in a U-shaped bend.

Inspecting Figs. 10 and 11, it is easy to see that the reflection of the shock wave near the external wall of the bend gives rise to a high pressure zone (Fig. 10, t = 0.1 ms) in which the self-ignition of the mixture occurred (bright spot at $x \approx 1.29$ m and $y \approx 0.03$ m in Fig. 11 at t = 0.1 ms). The self-ignition (secondary explosion) occurred at an angle of turn of about 50°–60°. It is seen that the instant of self-ignition nearly coincides with the instant of arrival of the rarefaction wave from the internal wall of the bend (expansion fans of pressure (Fig. 10) and density (Fig. 11) centered at the internal wall of the bend). By time t = 0.2 ms, the shock wave finished passing the U-bend while the self-ignition wave managed to have spread only through a narrow band along the external wall of the band (bright streak in Fig. 11 at t = 0.2 ms). Note that the self-ignition wave propagates both downstream and upstream. In addition, near the point of reflection of the shock wave from the external wall of the straight section of the channel behind the U-bend, a second self-ignition hotspot arises ($x \approx 1.20$ m, $y \approx 0.10$ m in Figs. 10 and 11 at t = 0.2 ms). At time t = 0.2 ms, the self-ignition

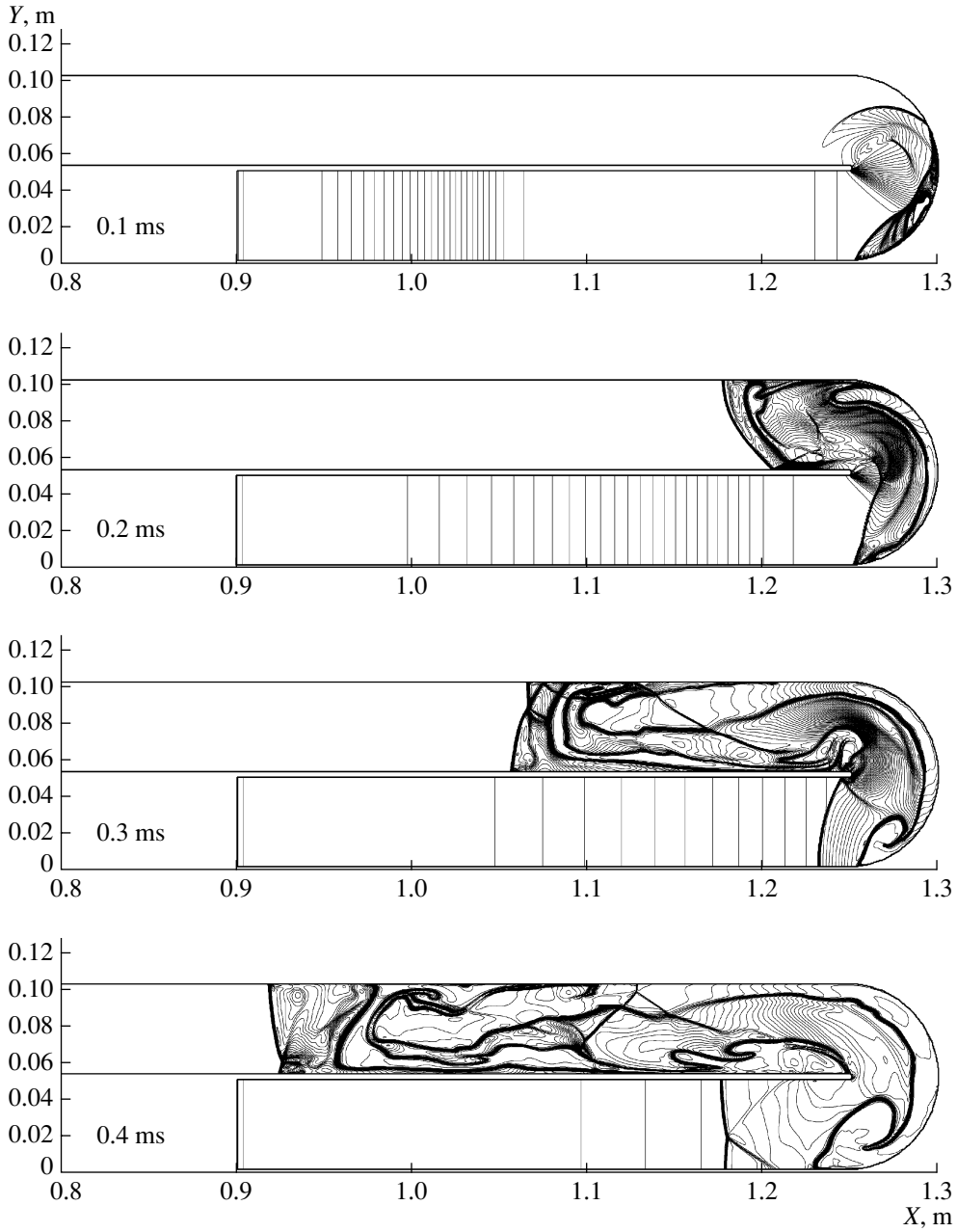

Fig. 11. Calculated density isolines at D = 1175 m/s and τ_+ = 0.3 ms.

wave propagating from this hotspot is seen to have spread over nearly the entire cross section of the channel, lagging behind the shock wave front by 1.5–2.0 cm, but without overlapping with the self-ignition wave from the first hotspot. Later (at t = 0.3 ms and t = 0.4 ms in Fig. 10 and 11), the distance between the shock wave front and the self-ignition wave front became larger, attaining 4–6 cm at t = 0.4 ms. Thus, in the first set of calculations, there were no prerequisites for detonation onset in the straight section behind the first U-bend. Note, however, that energy release continued behind the shock wave, thereby preventing it from rapid attenuation.

In the second set of calculations (Figs. 12 and 13), the self-ignition of the mixture occurred somewhat earlier than it did in the first set; therefore, the hotspot at t = 0.1 ms was larger (bright spot at ($x \approx 1.29$ m, $y \approx 0.03$ m in Fig. 13 at t = 0.1 ms). As in the first set of calculations, the propagation of the self-ignition wave occurred against the background of the cooling action of the rarefaction wave originating at the internal wall of the U-bend (expansion fans of pressure (Fig. 12) and density (Fig. 13) centered at the internal wall of the

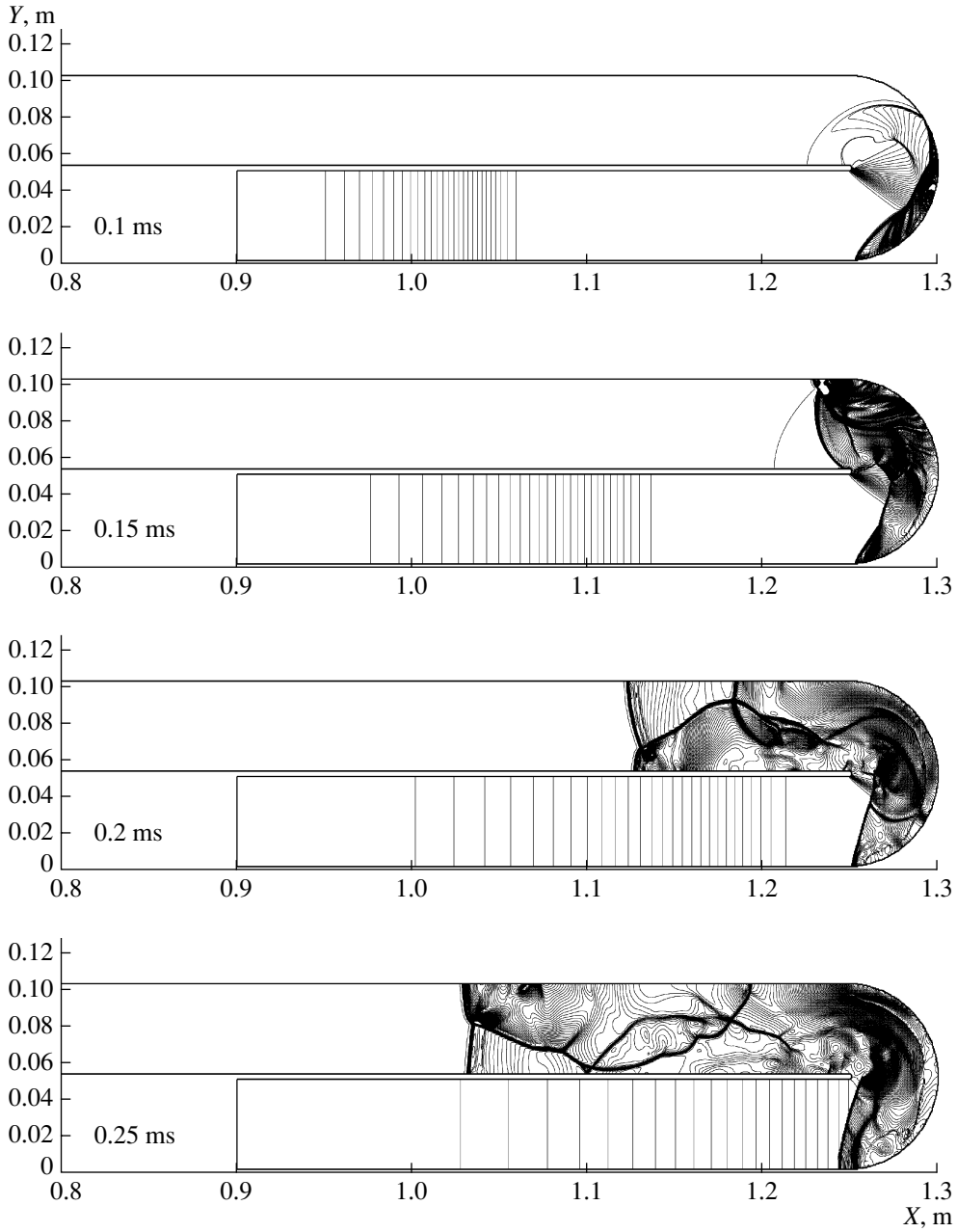

Fig. 12. Calculated pressure isolines at $D = 1200$ m/s and $\tau_+ = 0.3$ ms.

bend). Note, however, that, in contrast to the first set of calculations, at time $t = 0.15$ ms, the self-ignition wave is seen to have spread not only over a band along the external wall of the bend (bright streak in Fig. 13 at $t =$ 0.15 ms) but have obturated the entire cross section of the channel at the exit from the U-bend. The obturation occurred due to the secondary explosion near the point of reflection of the shock wave from the external wall at $x \approx 1.26$ m and $y \approx 0.10$ m (Figs. 12 and 13 at $t = 0.15$ ms) and the subsequent merge of the self-ignition waves from the first and second hotspots. At $t = 0.2$ and 0.3 ms, a detonation wave with a well-pronounced transverse wave and a reaction zone adjacent to the shock wave was propagating in the straight section of the channel behind the U-bend. Afterburning was observed at large distances from the detonation front.

Generally, the experimental and calculation results were found to be in close qualitative agreement. At the same time, quantitative deviations between the critical conditions of detonation onset are observed. This discrepancy can be explained by the distinctions in the geometries of U-bends of a cylindrical tube and a planar channel and by the use of a simplified kinetic scheme of propane oxidation.

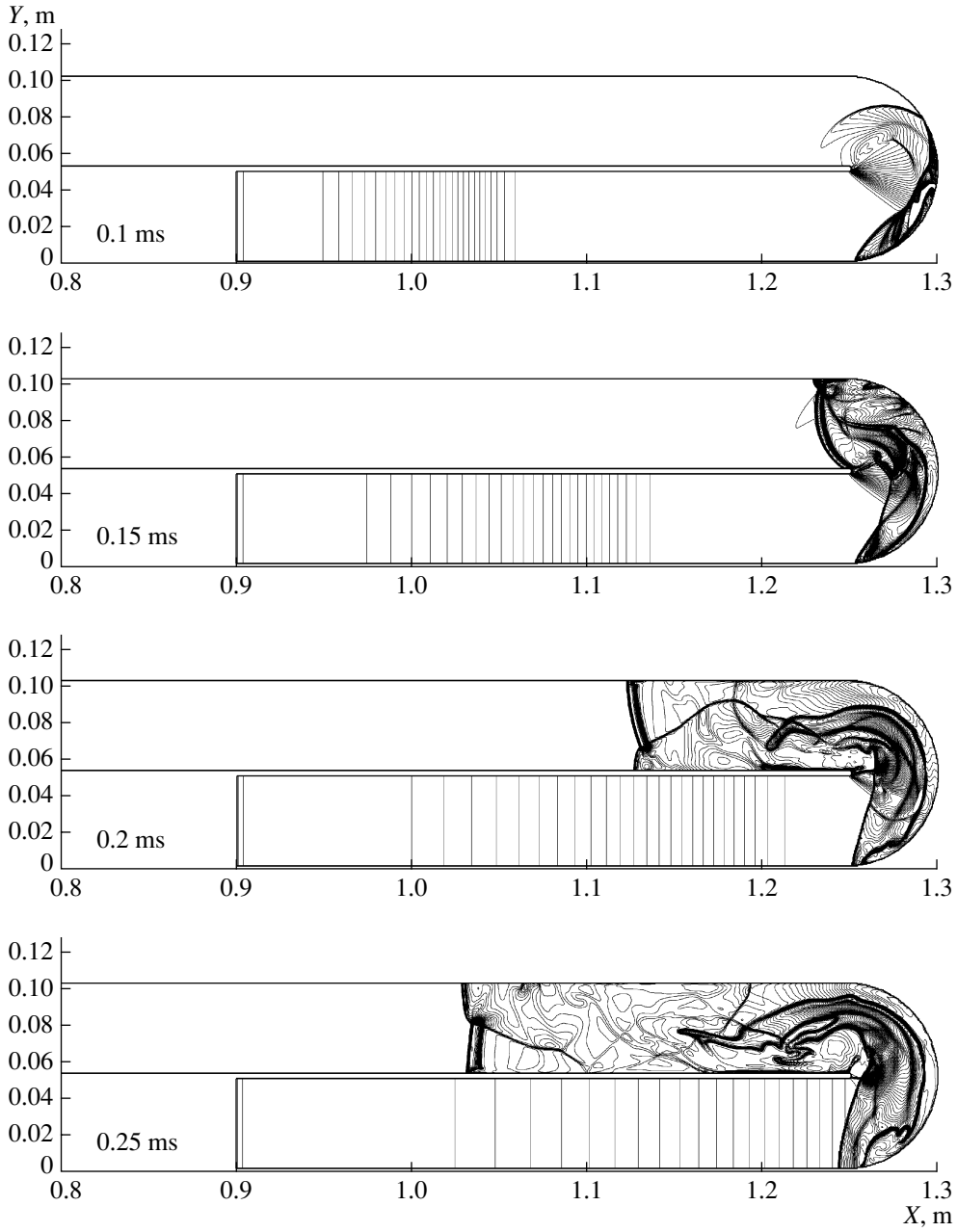

Fig. 13. Calculated density isolines at D = 1200 m/s and τ_+ = 0.3 ms.

In contrast to the propagation of a shock wave through a bend of a planar channel, the process in a bend of a cylindrical tube features additional reflections from lateral walls. In the latter case, the local values of pressure and temperature are expected to be higher while the initial Mach number, correspondingly, lower.

The one-step mechanism of propane oxidation used in our calculations is applicable only to describing the ignition delay time at high temperatures and, obviously, is not intended for modeling the process of combustion. In particular, it ignores the low-temperature oxidation of fuel and the dissociation of the combustion products.

CONCLUSIONS

Thus, in the present work, we performed systematic experimental and theoretical studies of the propagation of shock and detonation waves in cylindrical tubes and planar channels with two U-shaped bends of limiting curvature. It was experimentally demonstrated that such bends substantially facilitate the initiation of detonation in gases. The minimum shock wave velocity

required to initiate the detonation of a stoichiometric propane–air mixture under normal conditions in bent tubes 51 and 41 mm in diameter was found to be substantially lower (750–800 m/s) than the analogous value for straight tubes (1700–1800 m/s). Such waves can be readily generated in a straight tube with Shchelkin spiral with the help of a weak ignition source [9–11]. In this case, the detonation initiation mechanism is associated with the multiple reflections of the shock wave as it passes through bends and with secondary explosions. The results obtained can be used in designing air-breathing pulse detonation engines (ABPDEs) for aircrafts with a compact combustion chamber.

ACKNOWLEDGMENTS

This work was supported in part by the International Science and Technology Center (grant no. 2740) and Russian Foundation for Basic Research, project nos. 08-08-00068 and 05-08-50115.

I.O. Shamshin gratefully acknowledges the support of the Public Charitable Foundation for the Russian Science, program of the Ministry of Education and Science "Development of the Scientific Potential of Higher Education," and joint Russian–American program "Basic Research and Higher Education" under the auspices of U.S. Civilian Research and Development Foundation.

REFERENCES

1. E. E. Meshkov, Izv. Akad. Nauk SSSR, Ser. Mekh. Zhidk. Gaza, No. 5, 554 (1970).
2. K. Izumi, S. Aso, and M. Nishida, Shock Waves, No. 3, 213 (1994).
3. F. V. Shugaev, A. O. Serov, L. S. Shtemenko, et al., Shock Waves, No. 9, 31 (1999).
4. A. A. Borisov, B. E. Gel'fand, G. I. Skachkov, et al., Khim. Fiz. **7** (12), 1387 (1988).
5. B. E. Gelfand, S. V. Khomik, A. M. Bartenev, et al., Shock Waves, No. 10, 197 (2000).
6. H. Grönig, in *Proceedings of International Workshop on Shock Wave Focusing*, Ed. by K. Takayama (Tohoku Univ., Sendai, Jpn., 1990), p. 1.
7. M. A. Nettleton, *Gaseous Detonations: Their Nature, Effects, and Control* (Chapman and Hall, London, 1987).
8. S. M. Frolov, V. S. Aksenov, and I. O. Shamshin, in *Nonequilibrium Processes*, Vol. 1: *Combustion and Detonation*, Ed. by G. Roy, S. Frolov, and A. M. Starik (Torus Press, Moscow, 2005), p. 348.
9. S. M. Frolov, V. S. Aksenov, and V. Ya. Basevich, Dokl. Akad. Nauk **401** (2), 201 (2005) [Dokl. Phys. Chem. **401** (1), 28 (2005)].
10. S. M. Frolov, V. S. Aksenov, and V. Ya. Basevich, Teplofiz. Vys. Temp. **44** (2), 285 (2006).
11. S. M. Frolov, V. S. Aksenov, and I. O. Shamshin, in *Pulsed and Continuous Detonations*, Ed. by G. Roy, S. Frolov, and J. M. Sinibaldi (Torus Press, Moscow, 2006), p. 146.
12. S. M. Frolov, V. S. Aksenov, and I. O. Shamshin, Proc. Combust. Inst. **31**, 2421 (2007).
13. S. M. Frolov, *Pulsed Detonation Engines* (Torus Press, Moscow, 2006) [in Russian].
14. *JANAF Thermochemical Tables*, 2nd ed. (U.S. Dept. of Commerce, National Bureau of Standards, Washington, DC, 1970).
15. V. Ya. Basevich, A. A. Belyaev, and S. M. Frolov, Khim. Fiz. **17** (9), 112 (1998).
16. A. Burcat, K. Scheller, and A. Lifshitz, Combust. Flame **16** (3), 29 (1971).
17. A. A. Borisov, V. M. Zamanskii, V. V. Lisyanskii, et al., Khim. Fiz. **7** (5), 665 (1988).
18. S. B. Victorov, *Software for Equilibrium and Nonequilibrium Thermodynamic Calculations (Version 3.16)* (Semenov Institute of Chemical Physics, Moscow, 2002).
19. V. M. Kovenya and N. N. Yanenko, *Splitting Method in Problems of Gas Dynamics* (Nauka, Novosibirsk, 1981) [in Russian].
20. S. K. Godunov, A. V. Zabrodin, M. Ya. Ivanov, et al., *Numerical Solution of Multidimensional Problems in Gas Dynamics* (Nauka, Moscow, 1976) [in Russian].
21. V. P. Kolgan, Uchenye Zapiski TsAGI **3** (6), 68 (1972).
22. E. Hairer, S. P. Nörsett, and G. Wanner, *Solving Ordinary Differential Equations*, Vol. 1: *Nonstiff Problems* (Springer, Berlin, 1987; Mir, Moscow, 1990) [in Russian].
23. V. V. Azatyan, A. M. Kogan, M. G. Neigauz, et al., Kinet. Katal. **16** (3), 577 (1975).
24. I. O. Shamshin, Candidate's Dissertation in Mathematics and Physics (Moscow Inst. of Engineering Physics, Moscow, 2003).
25. B. E. Gel'fand, S. M. Frolov, and S. A. Tsyganov, Khim. Fiz. **8** (5), 1547 (1989).
26. V. A. Levin, V. V. Markov, T. A. Zhuravskaya, and S. F. Osinkin, in *Pulsed and Continuous Detonations*, Ed. by G. Roy, S. Frolov, and J. M. Sinibaldi (Torus Press, Moscow, 2006), p. 176.